Single-Phase Boost Inverter-Based Electric Vehicle Charger With Integrated Vehicle to Grid Reactive Power Compensation

Damith Buddika Wickramasinghe Abeywardana, *Member, IEEE*, Pablo Acuna, *Member, IEEE*, Branislav Hredzak, *Senior Member, IEEE*, Ricardo P. Aguilera, *Member, IEEE*, and Vassilios G. Agelidis, *Fellow, IEEE*

***Abstract*—Vehicle to grid (V2G) reactive power compensation using electric vehicle (EV) onboard chargers helps to ensure grid power quality by achieving unity power factor operation. However, the use of EVs for V2G reactive power compensation increases the second-order harmonic ripple current component at the DC-side of the charger. For single-phase, single-stage EV chargers, the ripple current component has to be supplied by the EV battery, unless a ripple compensation method is employed. Additionally, continuous usage of EV chargers for reactive power compensation, when the EV battery is not charging from the grid, exposes the EV battery to these undesirable ripple current components for a longer period and discharges the battery due to power conversion losses. This paper presents a way to provide V2G reactive power compensation through a boost inverter-based single stage EV charger and a DC-side capacitor without adversely affecting the EV battery. The operation of the boost inverter-based EV charger with second-order harmonic and switching frequency ripple current reduction, the dynamic behavior of the system, the transition between different operating modes, the DC-side capacitor voltage control above a minimum allowed voltage, and the DC-side capacitor sizing are extensively analyzed. The performance of the proposed system is verified using an experimental prototype, and presented results demonstrate the ability of the system to provide V2G reactive power compensation both with and without the EV battery.**

***Index Terms*—Electric vehicle (EV) charger, reactive power, second-order harmonic ripple current, vehicle to grid (V2G).**

I. Introduction

With the rapid depletion of fossil fuels and growing environmental concerns due to greenhouse gas emission, electric vehicles (EVs) have gained increased popularity. EVs utilize onboard or off-board chargers to charge the EV batteries from the electric grid [1]–[3]. The negative effects of EV charging on the power quality of low-voltage electricity distribution grids have been extensively studied in the technical literature, and it has been demonstrated that coordinated EV charging can mitigate adverse impacts such as increased peak load when large-scale EV grid integration is required [4]–[6]. Additionally, due to the energy storage capacity and vehicle to grid (V2G) operation capabilities, EVs can provide active and reactive power support to the electric grid either in battery-connected or disconnected mode [7]–[11].

The possibility of using EVs for reactive power support was extensively investigated in technical literature [10], [12]–[16]. Providing reactive power compensation using distributed energy storage devices, such as EVs, reduces the installation and maintenance costs associated with dedicated reactive power compensators such as capacitor banks, static VAR compensators, and static synchronous compensators [12]. However, the use of EVs for V2G reactive power compensation leads to additional concerns such as discharging of the battery and exposure of the battery to undesirable ripple current components. A second-order harmonic ripple current component at the DC-side of single-phase onboard EV chargers increases with V2G reactive power operation as explained in [14]. The adverse effects of the low-frequency ripple current components on the EV batteries can be mitigated using two stage charger topologies [2], [12]. However, according to the analysis presented in [14], a larger DC link capacitor has to be employed to handle the increased second-order harmonic ripple power requirement. For single stage EV chargers, the second-order harmonic ripple current has to be supplied by the EV battery unless a ripple compensation method is employed. Such continuous low-frequency ripple current components adversely affect the lifetime of battery due to internal heating [11], [17], and also increase the number of charge/discharge micro-cycles of the battery and, hence, deplete its lifetime more quickly [14], [18]. In addition to the second-order harmonic ripple current component, the EV battery has to withstand an undesirable switching frequency ripple current component for a longer period with V2G reactive power operation. Another significant concern of V2G reactive power compensation is discharging of the battery due to the

Manuscript received November 20, 2016; revised February 1, 2017 and April 3, 2017; accepted April 24, 2017. Date of publication May 3, 2017; date of current version January 3, 2018. Recommended for publication by Associate Editor C. K. Tse. *(Corresponding author: Damith Buddika Wickramasinghe Abeywardana.)*

D. B. Wickramasinghe Abeywardana, P. Acuna, and B. Hredzak are with the School of Electrical Engineering and Telecommunications, The University of New South Wales, Sydney, N.S.W. 2052, Australia (e-mail: damithabeywardana@yahoo.com; pabloacunarios@gmail.com; b.hredzak@unsw.edu.au).

R. P. Aguilera is with the School of Electrical, Mechanical and Mechatronic Systems, University of Technology Sydney, Sydney, N.S.W. 2007, Australia (e-mail: raguilera@ieee.org).

V. G. Agelidis is with the Department of Electrical Engineering, Danmarks Tekniske Universitet, Lyngby 2800, Denmark (e-mail: vasagel@elektro.dtu.dk).

Color versions of one or more of the figures in this paper are available online at http://ieeexplore.ieee.org

Digital Object Identifier 10.1109/TPEL.2017.2700944

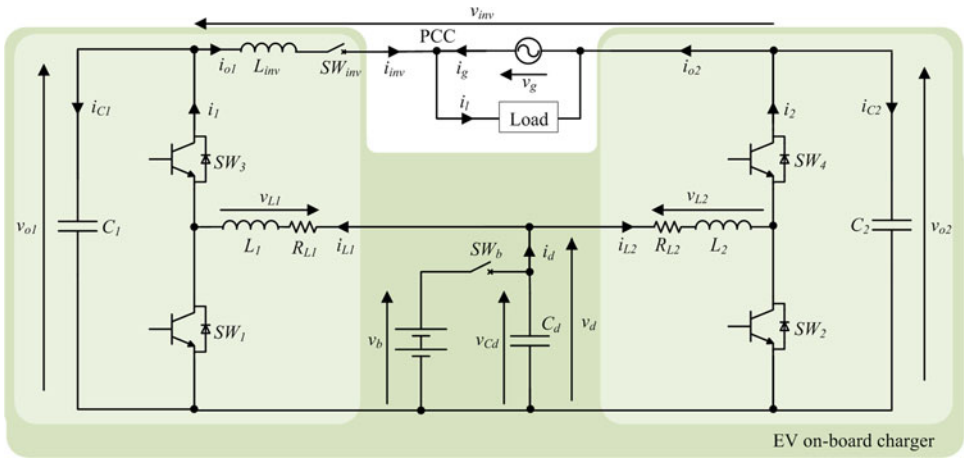

Fig. 1. Configuration of the boost inverter-based charger.

continuous operation of the power converter and associated power conversion losses [16]. In [13], the authors proposed to disconnect the EV battery from the charger, when it is not charging from the electric grid. The disconnection of the battery from the charger helps to avoid adverse impacts of V2G reactive power compensation on the EV battery. However, important effects related to the disconnection of the battery from the EV charger such as dynamic performance, capacitor sizing, and capacitor voltage control were not analyzed in [13].

Power electronic inverters play a key role in the EV battery storage systems. The boost inverter topology is a single-phase differential inverter topology that provides both boosting and inverting functions in a single power conversion stage [19], [20]. Various second-order harmonic ripple current reduction methods were studied for the single-phase boost inverter topology [21]–[24], and the current feedback ripple reduction method presented in [24] achieves a superior second-order harmonic ripple reduction performance. Furthermore, with the interleaved operation presented in [25], the boost inverter topology was able to reduce the switching frequency ripple component of the DC-side current. Due to the possibility of the boost inverter topology to provide both boosting and inverting functions in a single power conversion stage, and its capability of mitigating the second-order harmonic ripple component and switching frequency ripple component of the DC-side current, this topology becomes technically attractive in many DC energy storage system applications [19], [20], [24], [26]–[29].

In this paper, a boost inverter-based onboard EV charger for V2G reactive power compensation is presented. The DC-side current feedback method [24] and the interleaved operation [25] are adopted to mitigate the second-order harmonic ripple component and the switching frequency ripple component in the boost inverter DC-side current. When the battery is charging from the grid, the EV charger compensates for the reactive power requirement of the load through V2G reactive power operation. When the EV battery is not charging from the grid, due to coordinated EV charging control, it is proposed to disconnect the EV battery from the boost inverter. A DC-side capacitor is used to provide V2G reactive power compensation when the battery is disconnected. Practical recommendations related to V2G reactive power operation with the DC-side capacitor, the DC-side capacitor design, dynamic behavior, and capacitor voltage control above a minimum allowed voltage during transients are extensively analyzed and described. This analysis is a key to understand the practical control limitations of the V2G reactive power operation of the boost inverter-based EV charger when the EV battery is disconnected.

The main contributions of this paper can be summarized as follows. The paper presents a boost inverter-based EV charger with reduced second-order harmonic ripple and switching frequency ripple components in the EV battery current, which helps to increase the battery lifetime. As a way of further extending the battery lifetime, the possibility of disconnecting the EV battery when it is not charging from the grid and using a DC-side capacitor to provide V2G reactive power operation is studied. The dynamic performance of the system when the EV battery is disconnected from the inverter is studied and a DC-side capacitor selection method to maintain the DC-side capacitor voltage above a minimum allowed voltage is presented. The dynamic analysis and the capacitor selection methods are readily applicable for other inverter topologies. The proposed system, theoretical analysis, and design methods are validated using simulation and experimental results.

The paper is organized as follows. The operation of the boost inverter-based EV charger is presented in Section II. The DC-side capacitor energy controller and the DC-side capacitor selection are described in Section III. A design methodology for the boost inverter-based EV charger is discussed, and simulation and experimental results are presented in Section IV to validate the operation of the boost inverter-based EV charger. Finally, the conclusions of the paper are summarized in Section V.

II. Operation of the Boost Inverter-Based Charger

The system configuration of the interleaved boost inverter-based EV charger for V2G reactive power compensation is depicted in Fig. 1. The EV charger is connected to a single-phase AC grid through an interfacing inductor $L_{\rm inv}$. A reactive load is connected to the single-phase AC grid, and the EV charger is used to compensate for the reactive power component of the

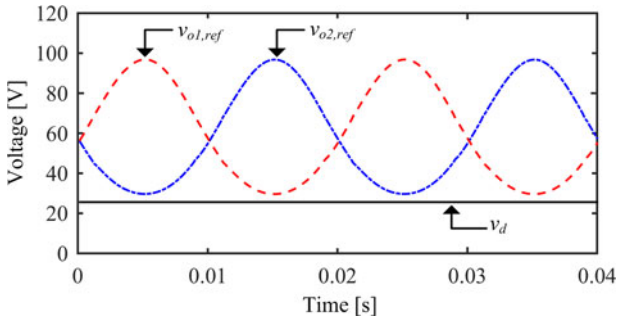

Fig. 2. Output capacitor voltage waveforms and boost inverter DC-side voltage.

load while charging the EV battery from the grid. When the EV is not charging from the grid, the switch SW_b is used to disconnect the EV battery from the boost inverter, and then the DC-side capacitor C_d is used to operate in the reactive power compensation mode.

The control objective of the boost inverter is to generate a sinusoidal voltage $v_{\rm inv}$, which follows the reference voltage

$$v_{\rm inv,ref} = V_{\rm inv}\sin(\omega t + \delta) \tag{1}$$

where $V_{\rm inv}$, ω, and δ are the amplitude, frequency, and phase angle of the inverter AC side voltage, respectively. The output capacitor voltages v_{o1} and v_{o2} are controlled to follow reference signals $v_{o1,\rm ref}$ and $v_{o2,\rm ref}$, where

$$v_{o1,\rm ref} = V_{\rm DC} + \frac{v_{\rm inv,ref}}{2} - Ki_{d,\rm AC} \tag{2}$$

$$v_{o2,\rm ref} = V_{\rm DC} - \frac{v_{\rm inv,ref}}{2} - Ki_{d,\rm AC}. \tag{3}$$

The differential output voltage between (2) and (3) produces the required inverter AC-side voltage as given in (1). The DC shift of the output capacitor reference voltages, $V_{\rm DC}$, is selected to ensure the boost mode operation of the converter legs (The minimum output capacitor voltage should be greater than the inverter DC-side voltage v_d). Hence, $V_{\rm DC}$ should be selected such that

$$\min(v_{o1,\rm ref}),\ \min(v_{o2,\rm ref}) \geq v_d \tag{4}$$

as shown in Fig. 2 [24]. The experimental prototype parameters summarized in Table I are used to obtain Fig. 2. As mentioned in the introduction, a DC-side current AC component feedback method proposed in [24] is adopted in this paper to mitigate the second-order harmonic ripple current component. Thus, in consideration of the null AC component of the boost inverter DC-side current ($i_{d,\rm AC}$) constraint, the third term in (2) and (3) can be considered as

$$-Ki_{d,\rm AC} = K(i_{d,\rm AC,ref} - i_{d,\rm AC}). \tag{5}$$

Hence, the third term can be seen as a proportional controller designed to control the DC-side current AC component to $i_{d,\rm ac,ref} = 0$. A detailed analysis of the second-order harmonic ripple current reduction using the DC-side current AC component feedback signal was presented in [24].

TABLE I
SIMULATION AND EXPERIMENTAL PARAMETERS

Variable	Simulation	Experimental
S	3 kVA (1 p.u.)	60 VA (1 p.u.)
V_g	325.27 V (1 p.u.)	60 V (1 p.u.)
ω	314.2 rad s^{-1}	314.2 rads^{-1}
$V_{\rm batt}$	140 V	25.6 V
$V_{\rm Cd,ref}$	140 V	25.6 V
$V_{\rm Cd,min}$	108 V	20 V
$V_{\rm DC}$	325 V	68 V
f_{sw}	20 kHz	20 kHz
C_1, C_2	35 μF	60 μF
L_1, L_2	480 μH	210 μH
$P_{\rm loss}$	96 W	11 W
$L_{\rm inv}$	11.8 mH (0.2 p.u.)	20 mH (0.2 p.u.)
R_{L1}, R_{L2}	0.12 Ω	0.2 Ω

The boost inverter-based EV charger is connected to a single-phase grid using an interfacing inductor L_g as shown in Fig. 1. The grid voltage v_g is given by

$$v_g = V_g\sin(\omega t). \tag{6}$$

The current supplied by the single-phase grid

$$i_g = I_g\sin(\omega t + \varphi) \tag{7}$$

and the current supplied by the inverter

$$i_{\rm inv} = I_{\rm inv}\sin(\omega t + \alpha). \tag{8}$$

The active power and the reactive power supplied by the boost inverter can be obtained as [30]

$$P_{\rm inv} = \frac{V_g V_{\rm inv}}{2\omega L_g}\sin\delta. \tag{9}$$

For small values of δ, the active power supplied by the boost inverter can be approximated as

$$P_{\rm inv} \approx \frac{V_g V_{\rm inv}}{2\omega L_{\rm inv}}\delta. \tag{10}$$

Moreover, the reactive power supplied by the inverter can be obtained as

$$Q_{\rm inv} = \frac{V_g V_{\rm inv}\cos\delta - {V_g}^2}{\omega L_g}. \tag{11}$$

For small values of δ, the reactive power supplied by the boost inverter can be approximated as

$$Q_{\rm inv} \approx \frac{V_g(V_{\rm inv} - V_g)}{2\omega L_{\rm inv}}. \tag{12}$$

According to (10) and (12), the active power supplied by the boost inverter can be controlled by modifying the inverter AC side voltage phase angle δ, and the reactive power supplied by the inverter can be controlled by modifying the inverter AC side voltage amplitude $V_{\rm inv}$. The active and reactive power control method was extensively discussed in literature [25], [27], [31] and tends to have a slow dynamic response. In order to increase the dynamic response of the active and reactive power controller, an interested reader can refer to the direct inverter output current control methods discussed in [29] and [32]. Furthermore, to reduce the size of the grid interfacing inductor, an *LC* filter can

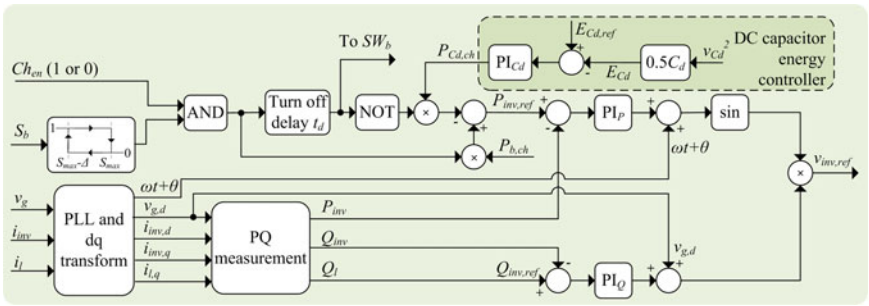

Fig. 3. Block diagram of the active and reactive power control system for the boost inverter-based charger.

be used as presented in [32]. In this paper, a grid interfacing inductor as shown in Fig. 1 is used, and a droop control method based on (10) and (12) is used to control the boost inverter output active and reactive power. The active and reactive power supplied from the boost inverter at the point of common coupling can be obtained using the *dq* components of the grid voltage v_g and the inverter AC-side current $i_{\rm inv}$ as

$$P_{\rm inv} = \frac{1}{2}\left(v_{g,d} i_{{\rm inv},d} + v_{g,q} i_{{\rm inv},q}\right) \tag{13}$$

$$Q_{\rm inv} = \frac{1}{2}\left(v_{g,q} i_{{\rm inv},d} - v_{g,d} i_{{\rm inv},q}\right). \tag{14}$$

In order to compensate for the reactive power of the load, the active and reactive power requirement of the load can be measured as

$$P_l = \frac{1}{2}\left(v_{g,d} i_{l,d} + v_{g,q} i_{l,q}\right) \tag{15}$$

$$Q_l = \frac{1}{2}\left(v_{g,q} i_{l,d} - v_{g,d} i_{l,q}\right). \tag{16}$$

The active and reactive power controller for the boost inverter-based charger is shown in Fig. 3. Before connecting the boost inverter to the grid, the inverter AC-side voltage is synchronized with the grid voltage using the phase lock loop shown in Fig. 3. Then, the switch $SW_{\rm inv}$ in Fig. 1 is used to connect the inverter to the single-phase grid. The PI controllers designed based on (10) and (12) are used to control the inverter output active and reactive power. A Ch_{en} signal is used to enable the charging of the EV battery from the grid, which can be generated from a coordinated EV charging algorithm [5], [10]. A hysteresis controller is used to maintain the SOC of the battery S_b less than a maximum allowable SOC value $S_{\rm max}$ as depicted in Fig. 3. When $Ch_{en} = 1$ and S_b is less than $S_{\rm max}$, the EV battery is connected to the boost inverter using SW_b. A mechanical switch can be used as the switch SW_b to avoid significant conduction and switching losses. Then, the EV battery is charged using a $P_{b,ch}$ active power reference. In order to compensate for the reactive power component of the grid connected load, the measured load reactive power using (16) is set as the reference to the inverter output reactive power. Two PI controllers are designed using (10) and (12) to control the active and reactive power supplied from the boost inverter to the grid.

When $Ch_{en} = 0$ or the EV battery SOC reaches its maximum value, the charging of the EV battery should be stopped. Note that, the battery should be disconnected from the charger when it is not charging from the grid to avoid discharging of the battery due to the power conversion losses. Furthermore, the disconnection of the battery from the inverter prevents the switching frequency current flow from the battery and also avoids the second-order harmonic ripple current component of the battery if a ripple reduction method is not employed. In order to stop the charging of the battery, the inverter power reference is set to zero. Due to the settling time of the inverter active power controller, the actual inverter active power takes some time to reach zero. If the EV battery is disconnected from the inverter, before the inverter output power reaches zero, the DC-side capacitor voltage will increase since it gets charged with the power absorbed from the grid. Due to the increased DC-side capacitor voltage, the inequality (4) may not be satisfied. In such situation, the minimum output capacitor voltage will saturate at the DC-side capacitor voltage. This will lead to a distorted inverter output voltage. This problem can be avoided by selecting a higher DC shift, $V_{\rm DC}$, for the output capacitor reference voltages, but a higher $V_{\rm DC}$ increases the required gain of the boost converter legs. Hence, it is important to delay the disconnection of the EV battery from the inverter until the active power absorbed by the inverter reaches zero. Hence, in this paper, it is recommended to disconnect the EV battery from the inverter after a predetermined time delay t_d using the switch SW_b. The turn-off time delay, t_d, can be selected according to the settling time of the inverter active power controller. When the EV battery is disconnected, the boost inverter can compensate for the grid load reactive power using the DC-side capacitor C_d.

When the battery is disconnected from the boost inverter, the stored energy of the DC-side capacitor has to be controlled to avoid the capacitor discharging. Hence, a DC-side capacitor energy controller as shown in Fig. 3 is used to control the stored energy of the capacitor at a reference value, and the PI controller for the energy controller has to be reset when the battery is disconnected from the converter.

III. Design of the DC-Side Capacitor and Capacitor Energy Controller

Fig. 4 illustrates the simplified block diagram of the DC-side capacitor energy controller, where $E_{Cd,\rm ref}$ is the capacitor energy level corresponding to the reference capacitor voltage value $v_{Cd,\rm ref}$. In Fig. 4, E_{Cd}, $E_{Cd,\rm init}$, $P_{\rm loss}$, and s are the stored energy in the DC-side capacitor, the initial stored energy in the DC-side capacitor, the power loss of the converter, and

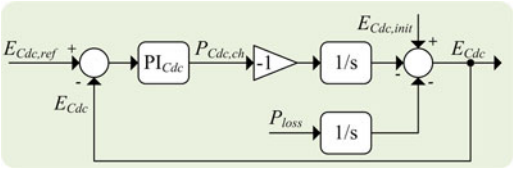

Fig. 4. Equivalent block diagram of the DC capacitor energy controller.

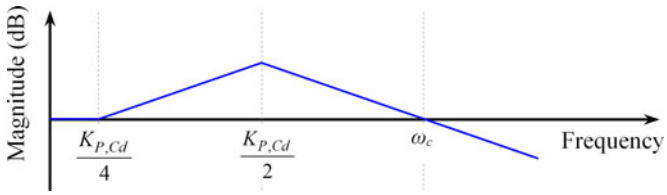

Fig. 5. Asymptotic bode plot of H_{ECd} when the system is critically damped.

the Laplace operator, respectively. A PI controller with a transfer function $H_{PI,Cd}$ is used in the capacitor energy controller, where

$$H_{PI,Cd} = K_{P,Cd} + \frac{K_{I,Cd}}{s} \tag{17}$$

and $K_{P,Cd}$ and $K_{I,Cd}$ are the proportional gain and the integral gain of the PI controller, respectively. Using Fig. 4, the transfer function between $E_{Cd,\mathrm{ref}}$ and E_{Cd} can be obtained as

$$H_{ECd} = \frac{E_{Cd}}{E_{Cd,\mathrm{ref}}} = \frac{K_{P,Cd}s + K_{I,Cd}}{s^2 + K_{P,Cd}s + K_{I,Cd}}. \tag{18}$$

Similarly, the transfer function between E_{Cd} and P_{loss}, H_{loss}, can be obtained as

$$H_{\mathrm{loss}} = \frac{E_{Cd}}{P_{\mathrm{loss}}} = \frac{-s}{s^2 + K_{P,Cd}s + K_{I,Cd}}. \tag{19}$$

The transfer function between E_{Cd} and $E_{Cd,\mathrm{init}}$ is

$$H_{\mathrm{init}} = \frac{E_{Cd}}{E_{Cd,\mathrm{init}}} = \frac{s^2}{s^2 + K_{P,Cd}s + K_{I,Cd}}. \tag{20}$$

The transfer function in (18) has a zero z and two poles p_1 and p_2, where

$$z = -\frac{K_{I,Cd}}{K_{P,Cd}}, \quad p_{1,2} = \frac{-K_{P,Cd} \pm \sqrt{{K_{P,Cd}}^2 - 4K_{I,Cd}}}{2}. \tag{21}$$

When ${K_{P,Cd}}^2 - 4K_{I,Cd} = 0$, the system is critically damped, and H_{ECd} can be rewritten as

$$H_{ECd} = \frac{E_{Cd}}{E_{Cd,\mathrm{ref}}} = \frac{(s + K_{P,Cd}/4)}{(s + K_{P,Cd}/2)^2}. \tag{22}$$

Using (22), an asymptotic Bode plot can be drawn as Fig. 5 and it can be observed that the gain cross-over frequency $\omega_c = K_{P,Cd}$. Hence, the proportional gain $K_{P,Cd}$ can be selected to control the bandwidth of the system given by (22).

When the battery is disconnected from the inverter, the DC-side capacitor has to supply the losses of the power converter; and hence, the stored energy in the DC-side capacitor drops. The reduction in the capacitor energy leads to a reduction in its voltage. The DC-side capacitor has to be selected to

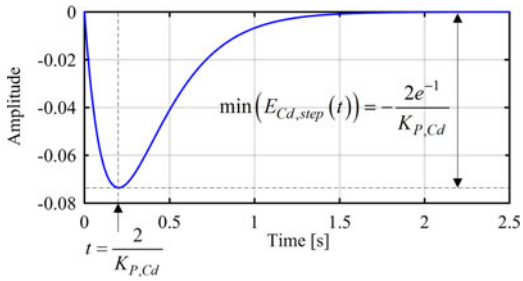

Fig. 6. Unit step response of H_{loss} when the system is critically damped.

maintain the capacitor voltage above a minimum value $v_{Cd,\min}$. For the critically damped system, the transfer function H_{loss} can be rewritten as

$$H_{\mathrm{loss}} = \frac{E_{Cd}}{P_{\mathrm{loss}}} = \frac{-s}{(s + K_{P,Cd}/2)^2}. \tag{23}$$

The unit step response of the transfer function H_{loss}, when the system is critically damped, is illustrated in Fig. 6. Using (23), the unit step response in time domain can be obtained as

$$E_{Cd,\mathrm{step}}(t) = -te^{-\left(\frac{tK_{P,Cd}}{2}\right)}. \tag{24}$$

The minimum value of (24) occurs when $t = 2/K_{P,Cd}$ and the minimum value is

$$\min\left(E_{Cd,\mathrm{step}}(t)\right) = -\frac{2e^{-1}}{K_{P,Cd}}. \tag{25}$$

Using (25), the DC-side capacitor energy change due to the converter power loss, P_{loss}, when the battery is disconnected from the inverter can be obtained as

$$\Delta E_{Cd,\mathrm{loss}} = \frac{-2e^{-1}}{K_{P,Cd}} P_{\mathrm{loss}}. \tag{26}$$

Then, the minimum required DC-side capacitor value to maintain its voltage greater than a critical minimum voltage $v_{Cd,\min}$ can be calculated as

$$C_{d,\mathrm{req}} = \frac{2\left|\Delta E_{Cd,\mathrm{loss}}\right|}{({v_b}^2 - {v_{Cd,\min}}^2)} \tag{27}$$

where v_b is the battery terminal voltage.

IV. Simulation and Experimental Study of the EV Charger

A. Design of the Control System for the Boost Inverter-Based EV Charger

The overall block diagram of the controller for the boost inverter-based EV charger is depicted in Fig. 7. In this paper, a double loop control strategy is used to control the boost inverter, and the outer voltage control loop and the inner current control loop for the left-hand side boost converter leg are shown in Fig. 8. The boost inverter AC-side reference voltage $v_{\mathrm{inv,ref}}$ is generated using the inverter active and reactive power controller depicted in Fig. 3. In order to reduce the second-order harmonic ripple component of the inverter DC-side current, the output capacitor reference voltages are controlled as in (2) and (3). A

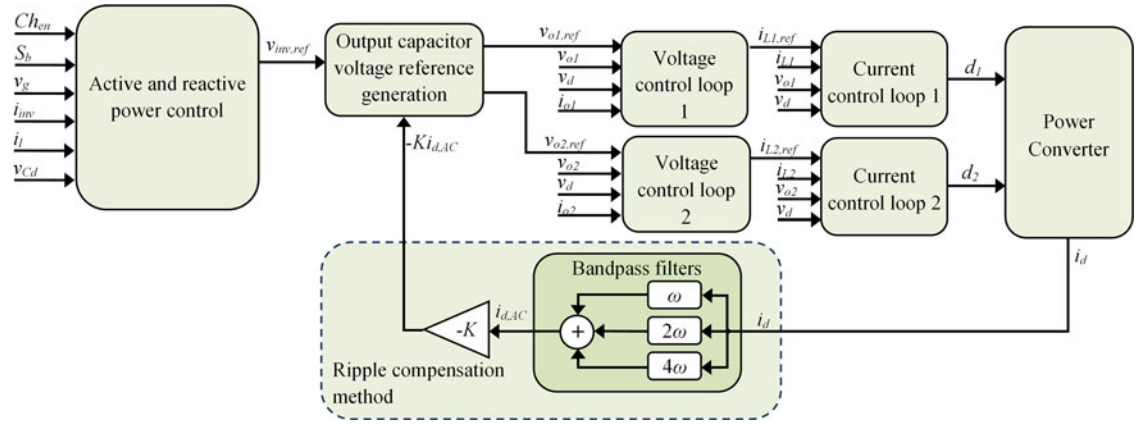

Fig. 7. Overall block diagram of the control system.

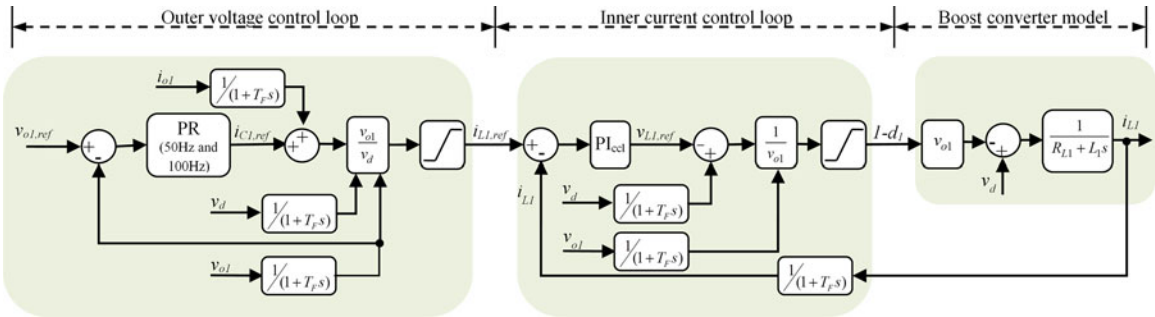

Fig. 8. Outer voltage control loop and inner current control loop for the left-hand side boost converter legs.

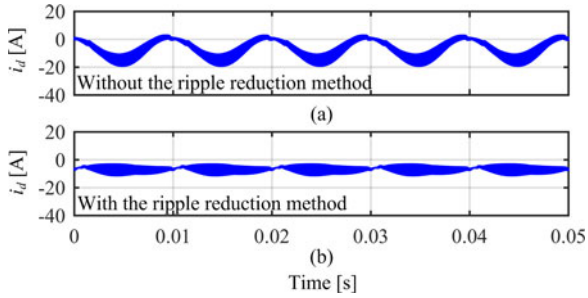

Fig. 9. Simulation waveforms illustrating the operation of the second-order harmonic ripple reduction method when the EV battery is charging from the grid and the EV charger provides the reactive power compensation. (a) inverter DC-side current waveform without the ripple reduction method and (b) inverter DC-side current waveform with the ripple reduction method.

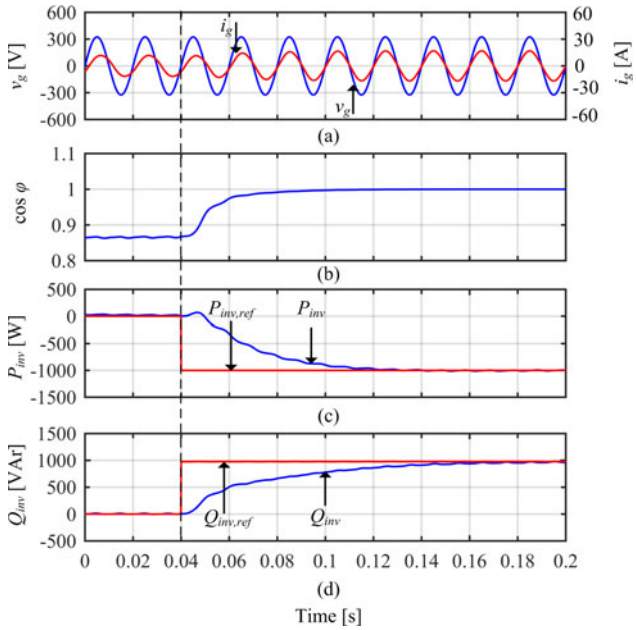

Fig. 10. Simulation waveforms of the boost inverter-based EV charger. (a) Grid voltage and grid current waveforms, (b) power factor between grid voltage and grid current, (c) active power waveform of the EV charger, and (d) reactive power waveform of the EV charger.

set of bandpass filters is used to obtain the AC component of the boost inverter DC-side current with minimum phase distortion and to block any DC component in the feedback path as shown in Fig. 7 [24]. In this paper, the feedback gain K is selected as 100, and a detailed explanation of the feedback gain selection for the ripple current reduction method is available in [24].

Fig. 8 illustrates the block diagram of the double loop controller for the left-hand side boost converter leg. A proportional-resonant controller with two resonant components at 50 and 100 Hz is used in the voltage control loop to achieve accurate sinusoidal voltage reference following [24]. The inner current control loops are designed using PI controllers. The outer voltage control loop bandwidth and the inner current control loop bandwidth are selected as 400 Hz and 4 kHz, respectively.

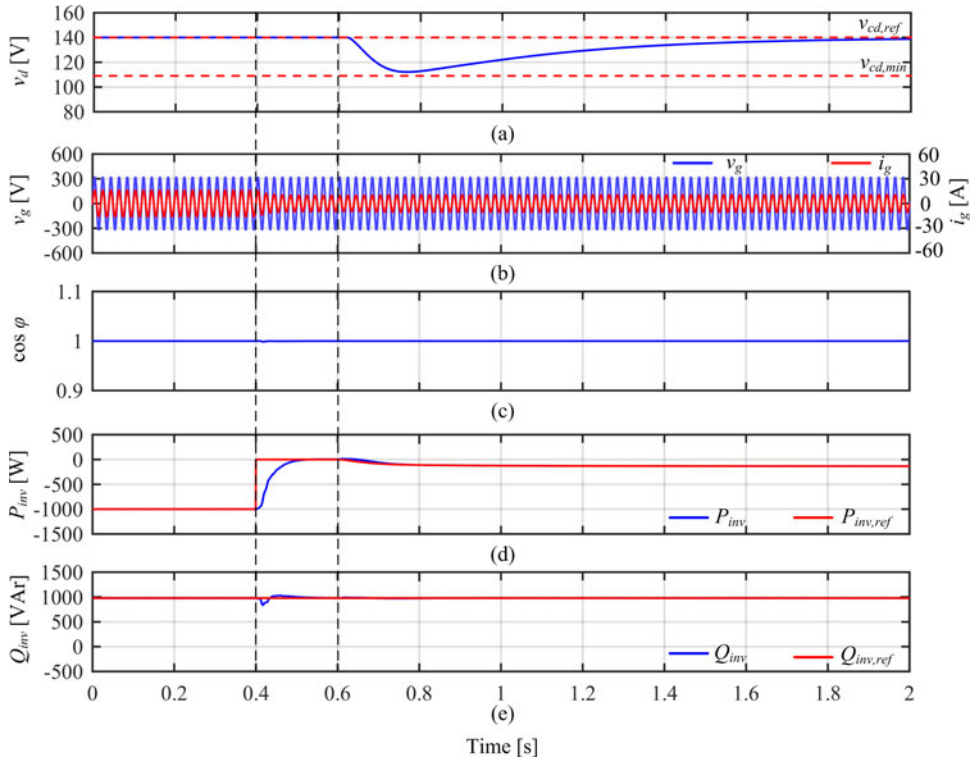

Fig. 11. Simulation waveforms illustrating operation of the boost inverter-based EV charger when the EV battery is disconnected from the charger at $t = 0.6$ s. (a) Grid voltage, the grid current, and the EV charger DC-side voltage, (b) power factor between the grid voltage and grid current, (c) active power waveform of the EV charger, and (d) reactive power waveform of the EV charger.

The analysis provided in Section III is used to design the DC-side capacitor energy controller. In this paper, the critically damped system is considered, and the proportional gain of the energy controller $K_{P,Cd}$ is selected as 10 to limit the bandwidth of the system given by (22) to 10 rad s^{-1}. Then, the integral gain $K_{I,Cd}$ is selected as 25 to obtain a critically damped system. The PI controllers PI_P and PI_Q are designed to obtain 0.1 s rise time approximately. Hence, the battery disconnection time delay t_d is selected as 0.2 s.

B. Simulation Study

A 3 kVA boost inverter-based EV charger and a 230 V single-phase AC grid are considered in the simulation study. The simulations were conducted using Matlab-Simulink with PLECS. The system parameters used for the simulations are summarized in Table I. The grid interfacing inductor and output capacitors for the simulation are selected to have the same per unit values as the experimental setup. However, the boost converter leg inductors L_1 and L_2 are designed to limit the switching frequency ripple component of the inductor current as explained in [25]. A series resistive-inductive load with 23.5 Ω resistance and 40 mH inductance is used as the equivalent load connected to the single-phase grid.

The operation of the second-order harmonic ripple reduction method when the EV battery is charging from the grid and the inverter is providing reactive power compensation for the grid load is presented in Fig. 9. The ripple reduction method reduced the second-order harmonic ripple current component from 8.198 to 0.522 A.

Fig. 10 demonstrates the operation of the EV charger in V2G reactive power compensation mode. At $t = 0.04$ s, the inverter is enabled to compensate for the load reactive power while charging as shown in Fig. 10. Here, $P_{\text{inv}} = -1$ kW. The inverter reactive power is controlled to compensate for the load reactive power as shown in Fig. 10(d). From Fig. 10(a) and (b), it can be seen that the grid voltage and the grid current are in phase after enabling the V2G reactive power compensation and the power factor reaches 1. The total harmonic distortion (THD) of the grid current when the inverter is compensating the load reactive power and charging the battery from the grid is obtained as 1.63%.

Then, a simulation test was conducted to evaluate the performance of the system, when the EV battery is disconnected from the inverter as shown in Fig. 11. The power loss of the inverter, P_{loss}, is measured and the energy change of the DC-side capacitor due to the converter losses $\Delta E_{Cd,\text{loss}}$ is calculated from (26) as 7.06 J. Then, the required DC-side capacitor value $C_{d,\text{req}}$ to maintain the DC-side voltage above the minimum value is calculated from (27) as 1780 μF. Fig. 11 illustrates the operation of the system when the battery is disconnected from the boost inverter at $t = 0.6$ s. Initially, the battery is charging from the grid while inverter provides the load reactive power compensation. From Fig. 11(b) and (c), the grid current and grid voltage waveforms are in phase, and the power factor is equal to 1. At $t = 0.4$ s, Ch_{en} signal set to zero in order to stop charging of

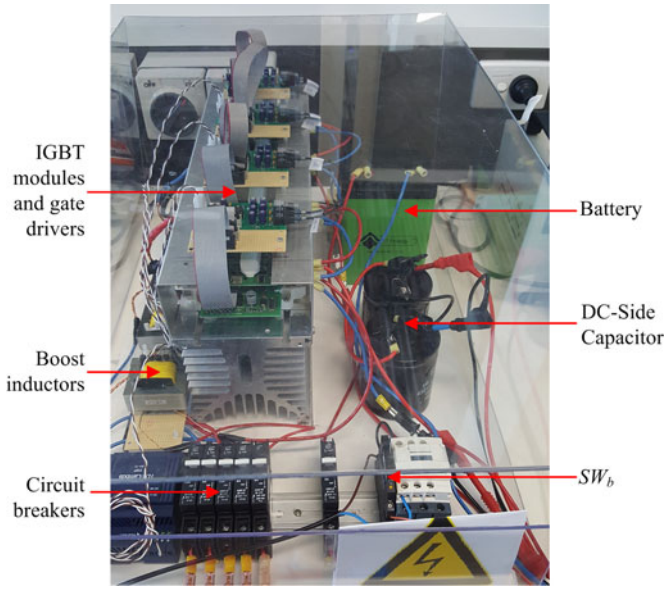

Fig. 12. Boost inverter-based EV charger experimental setup.

the battery, and hence, the active power reference is set to zero as shown in Fig. 11(c). After a t_d ($= 0.2$ s) time delay, the battery is disconnected from the inverter using the switch $SW_{\rm b}$. Due to the converter losses, a reduction in the DC-side capacitor voltage can be observed. The DC-side capacitor energy controller modified the inverter active power reference signal to maintain the capacitor voltage at the reference value. The selected DC capacitor energy controller parameters and the selected capacitor value ensure that the DC capacitor voltage is always greater than the minimum allowed voltage as shown in Fig. 11(a).

C. Experimental Results

The proposed boost inverter-based EV charger with V2G reactive power operation is verified using a low-voltage experimental setup shown in Fig. 12. The parameters of the power electronic converter are summarized in Table I, and the parameters are chosen to obtain similar per unit values as the simulation system. A 9.6-Ah 25.6 V $LiFePO_4$ battery is used in the experiment setup. The grid integration of the boost inverter-based EV charger is achieved using a step-up transformer. A series resistive–inductive load with 23.5 Ω resistance and 40 mH inductance is used as the equivalent load connected to the single-phase grid.

The operation of the second-order harmonic ripple current reduction method, when the EV battery is charging from the grid and the inverter is providing reactive power compensation for the grid load is presented in Fig. 13. Fig. 13(a) and (b) demonstrate the inverter DC-side current waveform without and with the ripple reduction method, respectively. The ripple reduction method reduced the second-order harmonic current component from 1.247 to 0.072 A. The second-order harmonic ripple amplitude of the DC-side current was measured using a Teledyne Lecroy HDO4054 500 MHz digital oscilloscope along with CP030A current probes (1-mA precision).

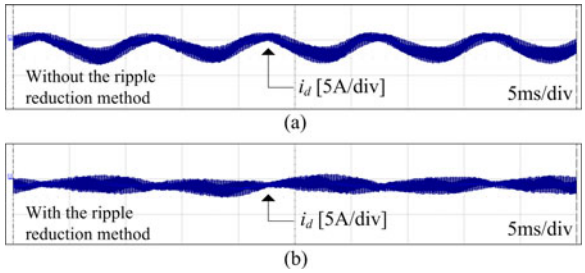

Fig. 13. Operation of the second-order harmonic ripple reduction method when the EV battery is charging from the grid and the EV charger provides the reactive power compensation. (a) Inverter DC-side current waveform without the ripple reduction method and (b) inverter DC-side current waveform with the ripple reduction method.

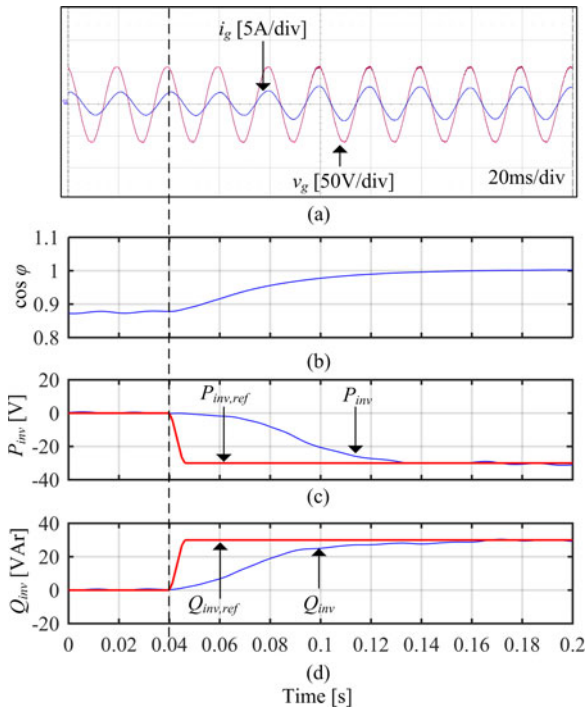

Fig. 14. Operation of the boost inverter-based EV charger. (a) Grid voltage and grid current waveforms, (b) power factor between grid voltage and grid current, (c) active power waveform of the EV charger, and (d) reactive power waveform of the EV charger.

Fig. 14 illustrates the operation of the boost inverter-based EV charger in the V2G reactive power operation mode. In this figure, the grid voltage and grid current waveforms were captured using a Teledyne Lecroy HDO4054 500 MHz digital oscilloscope, while the power factor, active power, and reactive power waveforms were captured using DSpace DS1006 system with 0.001-s sampling time. Initially, the boost inverter does not supply or absorb any active or reactive power as shown in Fig. 14(c) and (d). Due to the resistive–inductive load, the grid current i_g and the grid voltage v_g are not in phase. When $t = 0.04$ s, the boost inverter-based EV charger is enabled, and the inverter active power is controlled at $P_{\rm inv} = -30$ W as shown in Fig. 14(c) to charge the EV battery with a constant power. The inverter reactive power is controlled to compensate for the load reactive power as illustrated in Fig. 14(d). It can be observed

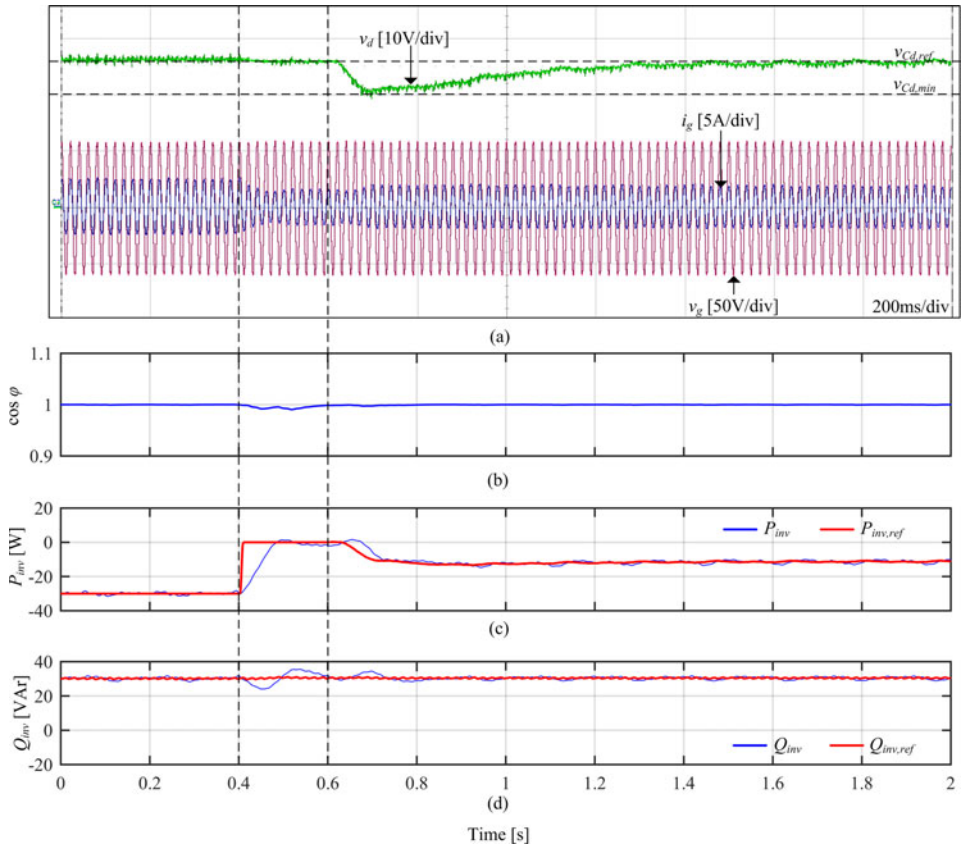

Fig. 15. Operation of the boost inverter-based EV charger when the EV battery is disconnected from the charger at $t = 0.6\,\mathrm{s}$. (a) Grid voltage, the grid current, and the EV charger DC-side voltage, (b) power factor between the grid voltage and grid current, (c) active power waveform of the EV charger, (d) reactive power waveform of the EV charger.

that due to the reactive power compensation, the grid voltage and the grid current are in phase as shown in Fig. 14(a) and the power factor reaches 1. Furthermore, the grid current THD when the inverter is supplying load reactive power compensation and charging the battery from the grid is obtained as 0.52%. A Teledyne Lecroy HDO4054 500 MHz digital oscilloscope with CP030A current probes was used to measure the harmonic content of the grid current. Up to the sixth-order harmonic component and 25 cycles were considered when calculating the THD values.

Next, the dynamic performance of the system, when the EV battery is disconnected from the inverter, is studied. The minimum allowed DC-side capacitor voltage is chosen as 20 V. The power loss of the inverter, P_{loss}, is measured, and the energy change of the DC-side capacitor due to the converter losses $\Delta E_{Cd,\mathrm{loss}}$ is calculated from (26) as 0.86 J. Then, the required DC-side capacitor value $C_{d,\mathrm{req}}$ to maintain the capacitor voltage above the minimum value is calculated from (27) as 6339 μF. Hence, a DC-side capacitor with 6600 μF is used in the experiments. Fig. 15 demonstrates the operation of the system when the battery is disconnected from the boost inverter at $t = 0.6\,\mathrm{s}$. Initially, the battery is connected to the inverter, and the boost inverter absorbs active power from the grid to charge the battery while compensating for the grid load reactive power component. Fig. 15(a) illustrates the inverter DC-side voltage v_d, grid voltage v_g, and grid current i_g. Due to the reactive power compensation, the grid voltage and the grid current waveforms are in phase, and the power factor is equal to 1 as shown in Fig. 15(b). At $t = 0.4\,\mathrm{s}$, Ch_{en} signal is set to zero in order to stop charging of the battery. Because of that, the active power reference signal for the boost inverter is set to zero as shown in Fig. 15(c). After a $t_d\ (= 0.2\,\mathrm{s})$ time delay, the battery is disconnected from the inverter using the switch SW_b. After the battery is disconnected from the grid, the DC-side capacitor starts to discharge due to the converter losses, and hence, a reduction in the DC-side voltage can be observed. Then, the DC-side capacitor energy controller modifies the inverter power reference signal $P_{\mathrm{inv,ref}}$ to maintain the DC-side capacitor voltage at the reference value as illustrated in Fig. 15(c). The selected DC capacitor energy controller parameters and the selected capacitor value ensure that the DC capacitor voltage is always greater than the minimum allowed DC capacitor voltage. Furthermore, the boost inverter-based EV charger allows obtaining the unity power factor through the whole test as shown in Fig. 15(a), (b), and (d).

V. Conclusion

In this paper, a single stage boost inverter-based EV charger with V2G reactive power compensation was proposed. The boost inverter topology allows EV battery charging using a single power processing stage. The topology extends the EV

battery lifetime by mitigating the second-order harmonic ripple current component and the switching frequency ripple current component at the DC-side of the inverter. To further extend the battery lifetime, the proposed charger allows disconnecting the EV battery from the EV charger when not charging from the grid and using a DC-side capacitor to provide the V2G reactive power compensation. The operation of the boost inverter-based EV charger when the EV battery is disconnected from the inverter was analyzed theoretically. This analysis is a key for selecting both the DC-side capacitor size and the controller parameters. The performance of the proposed system was verified using both simulation and experimental results. The presented simulation and experimental results illustrated the operation of the boost inverter-based EV charger and its capability to provide V2G reactive power compensation without adversely affecting the battery lifetime.

REFERENCES

[1] M. Yilmaz and P. T. Krein, "Review of battery charger topologies, charging power levels, and infrastructure for plug-in electric and hybrid vehicles," *IEEE Trans. Power Electron.*, vol. 28, no. 5, pp. 2151–2169, May 2013.

[2] S. S. Williamson, A. K. Rathore, and F. Musavi, "Industrial electronics for electric transportation: Current state-of-the-art and future challenges," *IEEE Trans. Ind. Electron.*, vol. 62, no. 5, pp. 3021–3032, May 2015.

[3] A. G. Boulanger, A. C. Chu, S. Maxx, and D. L. Waltz, "Vehicle electrification: Status and issues," *Proc. IEEE*, vol. 99, no. 6, pp. 1116–1138, Jun. 2011.

[4] Z. Luo, Z. Hu, Y. Song, Z. Xu, and H. Lu, "Optimal coordination of plug-in electric vehicles in power grids with cost-benefit analysis-Part II: A case study in china," *IEEE Trans. Power Syst.*, vol. 28, no. 4, pp. 3556–3565, Nov. 2013.

[5] J. Hu, S. You, M. Lind, and J. Ostergaard, "Coordinated charging of electric vehicles for congestion prevention in the distribution grid," *IEEE Trans. Smart Grid*, vol. 5, no. 2, pp. 703–711, Mar. 2014.

[6] Y. He, B. Venkatesh, and L. Guan, "Optimal scheduling for charging and discharging of electric vehicles," *IEEE Trans. Smart Grid*, vol. 3, no. 3, pp. 1095–1105, Sep. 2012.

[7] W. Kempton and S. E. Letendre, "Electric vehicles as a new power source for electric utilities," *Transp. Res. Part D: Transp. Environ.*, vol. 2, pp. 157–175, Sep. 1997.

[8] L. Cheng, Y. Chang, and R. Huang, "Mitigating voltage problem in distribution system with distributed solar generation using electric vehicles," *IEEE Trans. Sustain. Energy*, vol. 6, no. 4, pp. 1475–1484, Oct. 2015.

[9] H. N. T. Nguyen, C. Zhang, and M. A. Mahmud, "Optimal coordination of G2V and V2G to support power grids with high penetration of renewable energy," *IEEE Trans. Transp. Electrific..*, vol. 1, no. 2, pp. 188–195, Aug. 2015.

[10] V. Monteiro, J. G. Pinto, and J. L. Afonso, "Operation modes for the electric vehicle in smart grids and smart homes: Present and proposed modes," *IEEE Trans. Veh. Tech.*, vol. 65, no. 3, pp. 1007–1020, Mar. 2016.

[11] M. Yilmaz and P. T. Krein, "Review of the impact of vehicle-to-grid technologies on distribution systems and utility interfaces," *IEEE Trans. Power Electron.*, vol. 28, no. 12, pp. 5673–5689, Dec. 2013.

[12] M. C. Kisacikoglu, M. Kesler, and L. M. Tolbert, "Single-phase on-board bidirectional PEV charger for V2G reactive power operation," *IEEE Trans. Smart Grid*, vol. 6, no. 2, pp. 767–775, Mar. 2015.

[13] M. C. Kisacikoglu, B. Ozpineci, and L. M. Tolbert, "Reactive power operation analysis of a single-phase EV/PHEV bidirectional battery charger," in *Proc. IEEE 8th Int. Conf. Power Electron. ECCE Asia*, 2011, pp. 585–592.

[14] M. C. Kisacikoglu, B. Ozpineci, and L. M. Tolbert, "EV/PHEV bidirectional charger assessment for V2G reactive power operation," *IEEE Trans. Power Electron.*, vol. 28, no. 12, pp. 5717–5727, Dec. 2013.

[15] M. C. Kisacikoglu, B. Ozpineci, and L. M. Tolbert, "Effects of V2G reactive power compensation on the component selection in an EV or PHEV bidirectional charger," in *Proc. IEEE Energy Convers. Congr. Expo.*, 2010, pp. 870–876.

[16] M. Falahi, H. M. Chou, M. Ehsani, L. Xie, and K. L. Butler-Purry, "Potential power quality benefits of electric vehicles," *IEEE Trans. Sustain. Energy*, vol. 4, no. 4, pp. 1016–1023, Oct. 2013.

[17] S. Bala, T. Tengner, P. Rosenfeld, and F. Delince, "The effect of low frequency current ripple on the performance of a Lithium Iron Phosphate (LFP) battery energy storage system," in *Proc. IEEE Energy Convers. Congr. Expo.*, 2012, pp. 3485–3492.

[18] A. J. Ruddell *et al.*, "Analysis of battery current microcycles in autonomous renewable energy systems," *J. Power Sources*, vol. 112, pp. 531–546, Nov. 14, 2002.

[19] P. Sanchis, A. Ursaea, E. Gubia, and L. Marroyo, "Boost DC-AC inverter: A new control strategy," *IEEE Trans. Power Electron.*, vol. 20, no. 2, pp. 343–353, Mar. 2005.

[20] R. O. Caceres and I. Barbi, "A boost DC-AC converter: Analysis, design, and experimentation," *IEEE Trans. Power Electron.*, vol. 14, no. 1, pp. 134–141, Feb. 1999.

[21] Z. Guo-Rong, T. Siew-Chong, C. Yu, and C. K. Tse, "Mitigation of low-frequency current ripple in fuel-cell inverter systems through waveform control," *IEEE Trans. Power Electron.*, vol. 28, no. 2, pp. 779–792, Feb. 2013.

[22] Z. Guo-Rong, X. Cheng-Yuan, W. Hao-Ran, C. Wei, and T. Siew-Chong, "Dynamic characteristics of boost inverter with waveform control," in *Proc. 29th Annu. IEEE Appl. Power Electron. Conf. Expo.*, 2014, pp. 1771–1775.

[23] D. B. W. Abeywardana, B. Hredzak, and V. G. Agelidis, "A rule-based controller to mitigate DC-side 2nd-order harmonic current in a single-phase boost inverter," *IEEE Trans. Power Electron.*, vol. 31, no. 2, pp. 1665–1679, Feb. 2016.

[24] D. B. W. Abeywardana, B. Hredzak, and V. Agelidis, "An input current feedback method to mitigate the DC-side low frequency ripple current in a single-phase boost inverter," *IEEE Trans. Power Electron.*, vol. 31, no. 6, pp. 4594–4603, Jun. 2016.

[25] D. B. W. Abeywardana, B. Hredzak, and V. G. Agelidis, "Single-phase grid-connected LiFePO4 battery-supercapacitor hybrid energy storage system with interleaved boost inverter," *IEEE Trans. Power Electron.*, vol. 30, no. 10, pp. 5591–5604, Oct. 2015.

[26] D. B. W. Abeywardana, B. Hredzak, V. Agelidis, and G. Demetriades, "Supercapacitor sizing method for energy controlled filter based hybrid energy storage systems," *IEEE Trans. Power Electron.*, vol. 32, no. 2, pp. 1–1, Feb. 2017.

[27] J. Minsoo, M. Ciobotaru, and V. G. Agelidis, "A single-phase grid-connected fuel cell system based on a boost-inverter," *IEEE Trans. Power Electron.*, vol. 28, no. 1, pp. 279–288, Jan. 2013.

[28] J. Minsoo and V. G. Agelidis, "A minimum power-processing-stage fuel-cell energy system based on a boost-inverter with a bidirectional backup battery storage," *IEEE Trans. Power Electron.*, vol. 26, no. 5, pp. 1568–1577, May 2011.

[29] Z. Wei, D. D. C. Lu, and V. G. Agelidis, "Current control of grid-connected boost inverter with zero steady-state error," *IEEE Trans. Power Electron.*, vol. 26, no. 10, pp. 2825–2834, Oct. 2011.

[30] R. Teodorescu, M. Liserre, and P. Rodr´ıguez, *Grid Converters for Photovoltaic and Wind Power Systems*. New York, NY, USA: Wiley, 2011.

[31] J. C. Vasquez, R. A. Mastromauro, J. M. Guerrero, and M. Liserre, "Voltage support provided by a droop-controlled multifunctional inverter," *IEEE Trans. Ind. Electron.*, vol. 56, no. 11, pp. 4510–4519, Nov. 2009.

[32] W. Yao, X. Wang, P. Loh, X. Zhang, and F. Blaabjerg, "Improved power decoupling scheme for single-phase grid-connected differential inverter with realistic mismatch in storage capacitances," *IEEE Trans. Power Electron.*, vol. 32, no. 1, pp. 186–199, Jan. 2017.

Damith Buddika Wickramasinghe Abeywardana photograph and biography not available at the time of publication.

Pablo Acuna photograph and biography not available at the time of publication.

Branislav Hredzak photograph and biography not available at the time of publication.

Ricardo P. Aguilera photograph and biography not available at the time of publication.

Vassilios G. Agelidis photograph and biography not available at the time of publication.